

NICMOS Calibration Challenges in the Ultra Deep Field

Rodger I. Thompson

Steward Observatory, University of Arizona, Tucson, AZ 85721

Abstract. The reduction of NICMOS observations in the Hubble Ultra Deep Field required unique reduction and calibration techniques, not required for images containing brighter sources. This paper describes some of these techniques which may be useful in the reduction of other fields containing extremely faint sources. These techniques apply to NICMOS camera 3 which was the only NICMOS camera utilized in the observations. The absolute accuracy of the NICMOS camera 3 photometry was also investigated using the observations of the solar analog star P330-E. As a result the sensitivity of the camera in the F110W and F160W was found to be less than the sensitivities used in the construction of the Version 2.0 NICMOS Treasury catalog for the observations in the Hubble Ultra Deep Field. The catalog fluxes are too low by between 8 and 9%.

1. Introduction

In conjunction with the Director's Discretionary Time Advanced Camera for Surveys (ACS) observations of the Hubble Ultra Deep Field (HUDF) a Treasury Program of NICMOS images was conducted using the F110W and F160W filters in Camera 3. A detailed description of the data reduction and photometry is given in Thompson et al. (2005). This paper will elaborate on some procedures and contains additional calibrations obtained after the publication of Thompson et al. (2005). It is expected that the current treasury products (Version 2.0) will be amended to reflect the new calibrations. The treasury high level science products and processed images are available from the Multimission Archive at STScI (MAST). Due to the smaller size of the NICMOS camera 3 field of view only a subset of the ACS HUDF image was covered. We will refer to that field as the NICMOS Hubble Ultra Deep Field (NHUFD).

2. Observations

The NHUFD covers 5.4 sq. arc minutes roughly in the center of the HUDF. Equal observing time was allocated to the F110W and F160W filters. Each orbit produced one 1344 second integration in each of the filters. The F110W observation always preceded the F160W integration. The orientation was chosen to be as close to the orientation of the ACS images as possible. The observing period was divided into two epochs with the NICMOS orientations clocked by 90 degrees between the two epochs. The STScI scheduler was able to make all orbits free of SAA passages which greatly simplified the data reduction. The images were taken in a 3x3 grid and dithered to reduce the effects of intrapixel sensitivity variations. The final F110W and F160W images supplied to MAST are 144 arc seconds on each side. See Thompson et al. (2005) for further details.

3. Photometric Challenges of the NHUDF

Although the NICMOS images did not reach the depth of the ACS images due to the reduced observing time per unit area, they did reach a level that required special reduction techniques. To characterize the sensitivity the 1σ noise flux is 4.6×10^{-9} Jy per pixel which is equivalent to 1 detected photon every 450 seconds which is an average of 3 detected photons per integration. One analog to digital converter unit (ADU) is 6.5 electrons therefore the 1σ level is 0.5 ADUs per integration. These signals are superimposed on a sky signal due to zodiacal light of 1 detected photon per second.

4. Dark Images

The NICMOS dark current images have very significant structure, often referred to as shading. This structure has an amplitude that is much larger than the signals due to faint galaxies, therefore, proper subtraction of accurate dark images is essential for proper reduction of the NHUDF images. The dark images are also temperature dependent so that even small changes in the detector temperature can alter the dark structure. To ensure proper dark images, a dark image was taken in each NHUDF orbit during the occultation period of the orbit. The dark images were then medianed to produce an accurate dark image that was contemporaneous with the science images for each read in the SPARS64 multiaccum readout sequence.

There was some concern about the darks since the temperature set point of the NICMOS Cooling System (NCS) was changed during the course of the observations to adjust for seasonal changes of the heat load on HST. Examination of the darks previous to the set point change and after the change did not reveal any significant differences.

5. Bad Pixels

Bad pixels are usually defined as pixels with less than 10% of the response of average pixels or hot pixels with dark currents that make them nonlinear after 1000 seconds of integration. For the NHUDF this definition was expanded to include a more stringent limit on the allowed dark current. The more stringent definition increased the number of bad pixels from 170 to 1012. This still, however, left warm pixels with significant dark current. This dark current varied with detector temperature and had significant poisson variation compared to the galaxy flux. After dark image subtraction these pixels often produced either spikes or holes in the images, depending on whether their temperature change and poisson error made them higher or lower than the median represented by the dark image. These pixels usually appeared as singular high contrast dark or bright spots.

These pixels are identified by comparing their contrast to the surrounding pixels with the maximum contrast in the well known NICMOS Point Spread Function (PSF). In a single image a pixel value was declared bad if all three of the following criteria were met.

1. The value of the pixel is greater than the 3σ noise value
2. Its contrast relative to the 8 surrounding pixels is higher than the maximum contrast from a centered point source.
3. The average value of the surrounding pixels was less than a preset number of σ .

The last criterion was established so that the centers of unresolved galaxies were not corrected if poisson noise increased their contrast above the maximum contrast of the PSF.

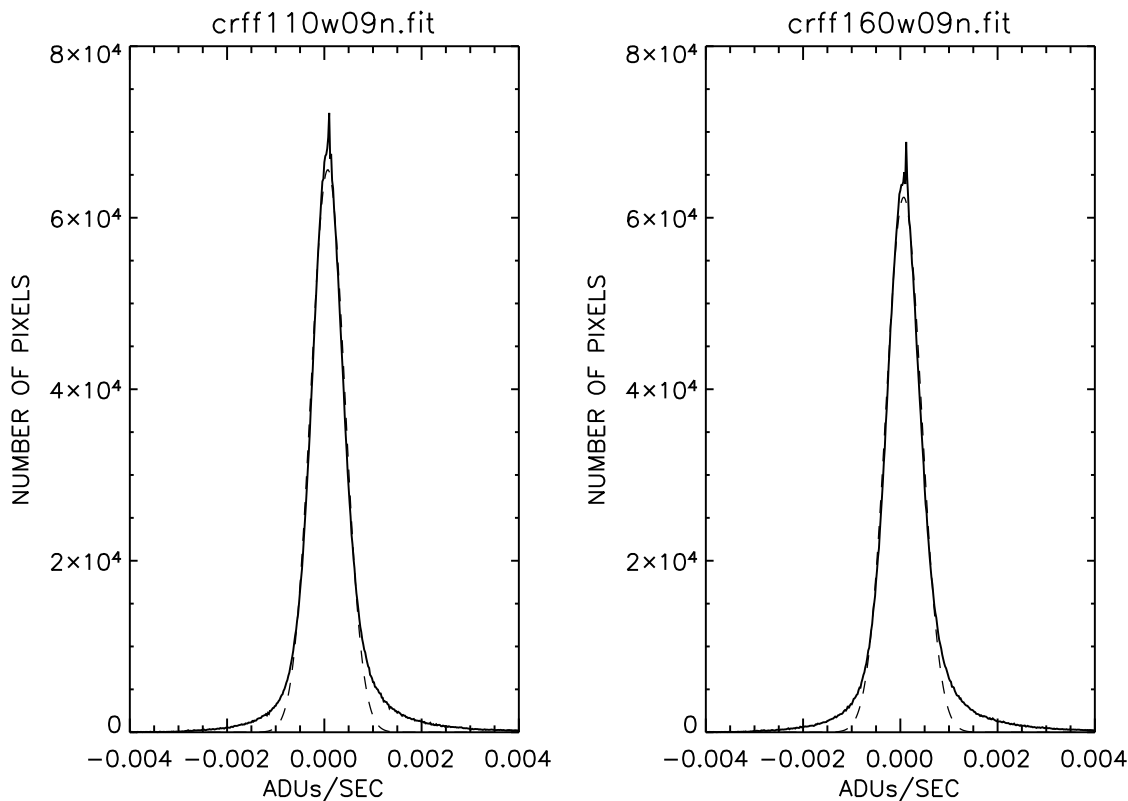


Figure 1: This is the distribution of pixel values for the F110W and F160W images in ADUs/sec. along with a Gaussian fit to the distribution shown by the dashed line. The long positive tail on each distribution is the contribution from real sources.

6. Quadrant Bias Removal

The NICMOS detectors are divided into 4 quadrants of 128x128 pixels, each with an independent readout amplifier. This was done to provide redundancy against amplifier failure. This sometimes results in a phenomenon called quadrant bias which is a DC offset of the voltages of all pixels in a detector quadrant. If there is an offset, the flat field correction imprints its pattern into the DC bias. The flat field correction function has significant power on small spatial scales which can be detected by a procedure developed by Mark Dickinson and described in the HST NICMOS data handbook (Mobasher et al. 2004). The procedure adds and subtracts a range of DC offsets to the image before the flat field procedure. The fluctuations in the image are measured after the flat field is applied and the offset that produces the minimum fluctuation is used to correct the quadrant bias. The fluctuation is measured by the FWHM of the distribution of all pixel values. Figures 1 and 2 show the distribution of pixel values and the fluctuation distribution measured by a Gaussian fit to the pixel value distribution for a typical image in the NHUDF.

This procedure works well for images that contain faint objects and where the majority of pixels are background. Figure 1 shows that this is the case for the NHUDF. For images with bright objects the quadrant bias offsets may not be significant.

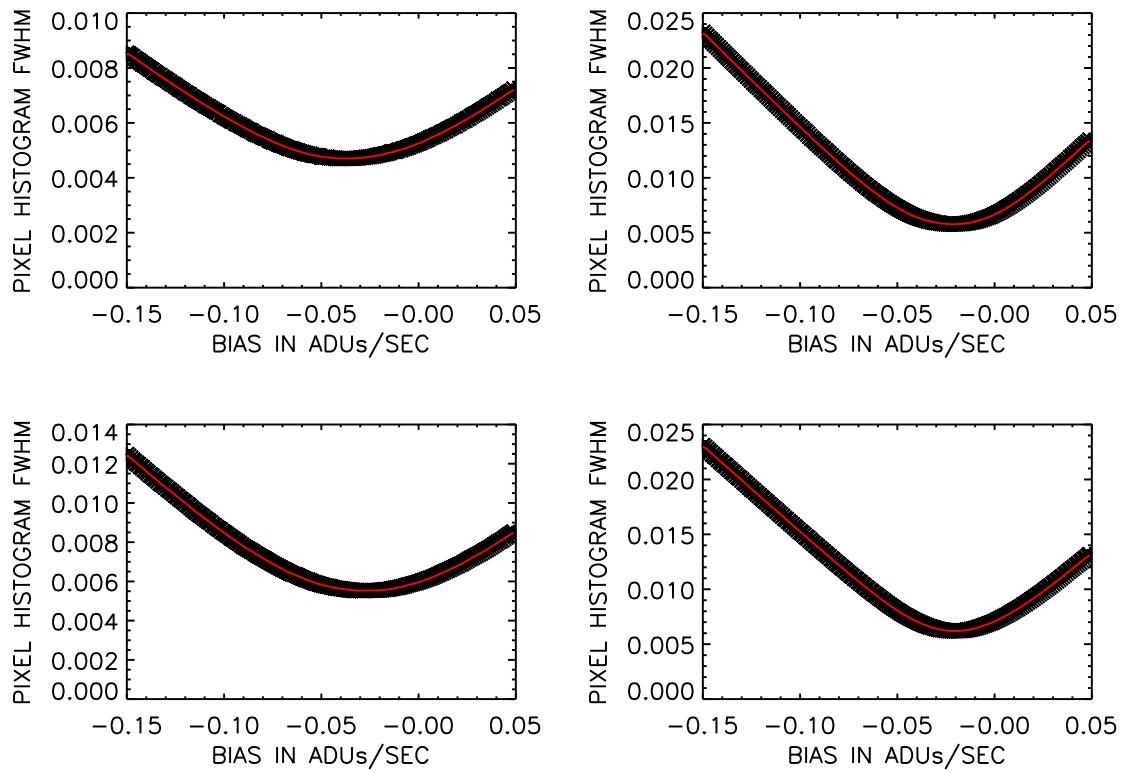


Figure 2: This shows the value of the fluctuations as measured by the FWHM of the pixel value distribution versus the offset applied in the quadrant bias removal procedure.

7. Background Subtraction

As discussed in Section 3 the sky background flux is higher than the fluxes from the majority of objects and much higher than the 1σ fluxes. Careful background subtraction is therefore very important for detecting objects and for accurate photometry. The primary source of the background is zodiacal light which is primarily reflected light rather than thermal emission at the NICMOS wavelengths. The background is determined by taking a median of all of the images in a filter. The 3x3 tiling and the dithering of images at each tile position ensures that the median measures the smooth background rather than the average of the source flux. The median produced by this procedure is very flat and shows no trace of source structure to the noise limit of the image. Since the zodiacal flux is time and position variable, the median background images were produced for each of the two epochs of observation. The background image was subtracted from each image before the images were combined in the drizzle process.

8. SAA Persistence

In general SAA persistence is an important problem for the observation of faint objects. Correction methods for images with persistence have been developed by STScI and are described in the NICMOS handbook. The NHUDF, however, benefited from an excellent scheduling effort by Beth Perriello and did not have any SAA impacted orbits. Occasional large cosmic ray hits did occur and were generally handled by masking out the affected areas of the image as discussed in sections 9. and 10..

9. Visual Inspection

Before the images were drizzled all 288 (144 F110W and 144 F160W) were visually inspected over a range of stretches for any artifacts that might affect the quality of the final image. The most common artifacts found in the images were persistent images from cosmic rays and satellite passages through the field of view. The cosmic ray events appear to be showers from high energy protons impacting the instrument and producing an intense shower of byproducts that affect a large area of the detector. Less than 10 images per filter were affected by this phenomenon. This is a very important step in the analysis due to the order of the integrations during an orbit. Each orbit contains a F110W image followed by a F160W image. A cosmic ray hit before the start of integrations in an orbit will produce a persistent image that will be strongest in the F110W image and will have faded to produce a weaker F160W image. The result will be an optical dropout source with a blue F110W to F160W color, the signature of a high redshift source. Every optical dropout candidate was inspected to make sure that the resultant flux did not come from such a single event. This resulted in the elimination of one source that appears in the Treasury Version 1 images but is removed from the Version 2 images. In addition any obvious noise sources were also identified.

10. Masking

All artifacts identified by visual inspection or other means were masked out in the images where they occurred by setting the flux to zero and setting the weight to zero in the drizzle process. In addition to the individual image masks the bottom 15 rows of all of the images were masked out. This region suffers slight vignetting which is of no consequence in most images but produces a region of significantly higher noise in these images. A small triangular region in the upper right hand corner of all images was also masked out. This is

a region of strongly varying pixel response which again has negligible effect in most images but produces a higher noise region in the NHUDF images. The common mask and the individual image masks are part of the NHUDF Version 2 data set available from MAST. It is highly recommended that any use of the NHUDF images for statistical purposes should take into account the varying weight across the images. This is mainly due to the variance in detector sensitivity but is also affected by the masked area.

11. Photometric Accuracy

Photometric accuracy of the images is extremely important, particularly for those studies that match template Spectral Energy Distributions (SEDs) to the combination of ACS and NICMOS measurements in the HUDF. There are also discussions of the photometric accuracy of NICMOS in other contributions to these proceedings (see the contributions by deJong and Mobasher).

11.1. Relative Accuracy

The relative accuracy of the NHUDF images is defined as the relative accuracy between the fluxes of objects in an image and the accuracy of the F110W to F160W color. The dithering and tiling has smoothed out the large QE variations in the NICMOS camera 3 detector, however, that is already well handled by the flat field correction. More importantly the dithering has mitigated the effect of intra pixel QE variations. This results in a relative accuracy of better than 5% with some areas of high signal to noise having significantly better accuracy.

11.2. Absolute Accuracy

Presentations and discussions at the workshop raised questions about the absolute calibration of the camera 3 F110W and F160W filters. As a result of this discussion the author revisited the initial calibration, particularly in light of the much more extensive standard star observations that are available now, which were not available at the time of the initial calibration. This is material that was not presented at the workshop but is an important contribution to NICMOS calibration and is therefore included in the proceedings. As a result of the work below the new calibration of the NICMOS camera 3 F110W and F160W filters gives the sensitivity of the F110W band as 1.70×10^{-6} Janskys per ADU per second and the F160W band as 2.06×10^{-6} Janskys per ADU per second. This means that a star with a Vega spectrum will have that flux in Janskys at the effective wavelength of the filters which are 1.103 and 1.595 microns respectively for the F110W and F160W filters.

11.3. New Photometric Analysis

The recalibration utilizes the observations of the solar analog star P330-E since the installation of the NCS in February of 2003. The star is assumed to have the same spectrum as the solar spectrum determined by Thuillier et al. (2003). The calibration also assumes that the photometric data on Vega by Campins, Rieke and Lebofsky (1985) and Bessell (1990) are correct.

P330-E is one of the solar analog stars observed by Persson et al. (1998) as part of the calibration program for NICMOS. The first step in the calibration process is the calculation of the effective wavelength of the Persson and NICMOS filters. The effective wavelength is defined by

$$\lambda_e = \frac{\int \lambda T(\lambda) d\lambda}{\int T(\lambda) d\lambda} \quad (1)$$

where $T(\lambda)$ is the transmission of the filter only and does not include the quantum efficiency of the detector. The effective wavelengths of the Persson filters were calculated from the transmission functions given in Persson et al. (1998) and the NICMOS effective wavelengths from the measured transmission of the filters before flight. Table 1 gives the measured values of the effective wavelengths.

Table 1: The effective wavelengths of the filters in microns.

Filter	Persson J	Persson H	Persson K	NICMOS F110W	NICMOS F160W
Effective λ	1.24	1.554	2.257	1.103	1.595

The quantum efficiency of the Persson observation detector was measured by hand from Figure 4 of Persson et al. (1998) and multiplied by the filter transmission to produce the response functions of the Persson system.

The next step was the transfer of the Campins et al. (1998) and Bessell (1990) photometry to the Persson system by fitting the Campins and Bessell photometry with a cubic spline fit and calculating the expected signal using the Persson response function. The Persson 0 magnitude values were found to be 1606, 1019 and 644 Janskys for J, H and K taking into account the 0.02 magnitude difference between the Arizona and Persson systems.

Using the Persson measurement of P330-E the flux at the effective wavelengths was determined. These fluxes, along with the scaled fluxes of the Thuillier et al. (2003) solar spectrum are listed in Table 2. The Thuillier et al. (2003) solar spectrum has some differences from the previously used solar analog spectrum as is shown in Figure 3.

Table 2: P330-E photometry and the scaled solar flux to match it.

Filter	P330-E (Jy)	Solar (Jy)
J	3.077×10^{-2}	3.138×10^{-2}
H	2.53×10^{-2}	2.453×10^{-2}
K	1.749×10^{-2}	1.756×10^{-2}

The scaled solar spectrum was then integrated over the F110W and F160W response function to determine the expected number of ADUs per second from the star. These values were then compared to the P330-E observations from proposal IDs 9325, 9639, 9995, and 10381 which together contain 182 observations of the star in the F110W and F160W filters with camera 3. To eliminate background flux a median of all 182 images was taken and then subtracted from the individual images. The median was inspected for any residual source flux and none was found since the location of the image was essentially randomly placed between the images.

The median subtracted images were then analyzed using SExtractor (SE) with 5 different photometric apertures of 2.7, 5, 8, 15 and 30 pixels. The pixels are 0.02 arc seconds in size. The smallest aperture was chosen to match the smallest aperture in the Version 2 Treasury data for the NHUFD. Initially an 80 pixel aperture was also used but its flux was identical within the noise to the 30 pixel aperture indicating that all of the flux was included in the 30 pixel aperture. Table 3 gives the aperture functions derived from these measurements and Figure 4 shows the functions.

Based on these measurements the sensitivity of the F110W filter was reduced by a factor of 0.925 and the sensitivity of the F160W filter by 0.910. The F110W and F160W fluxes in the Version 2 Treasury NHUFD should be increased by the inverse of these reductions. It should be noted that the aperture fluxes listed in the catalog are strictly the flux observed

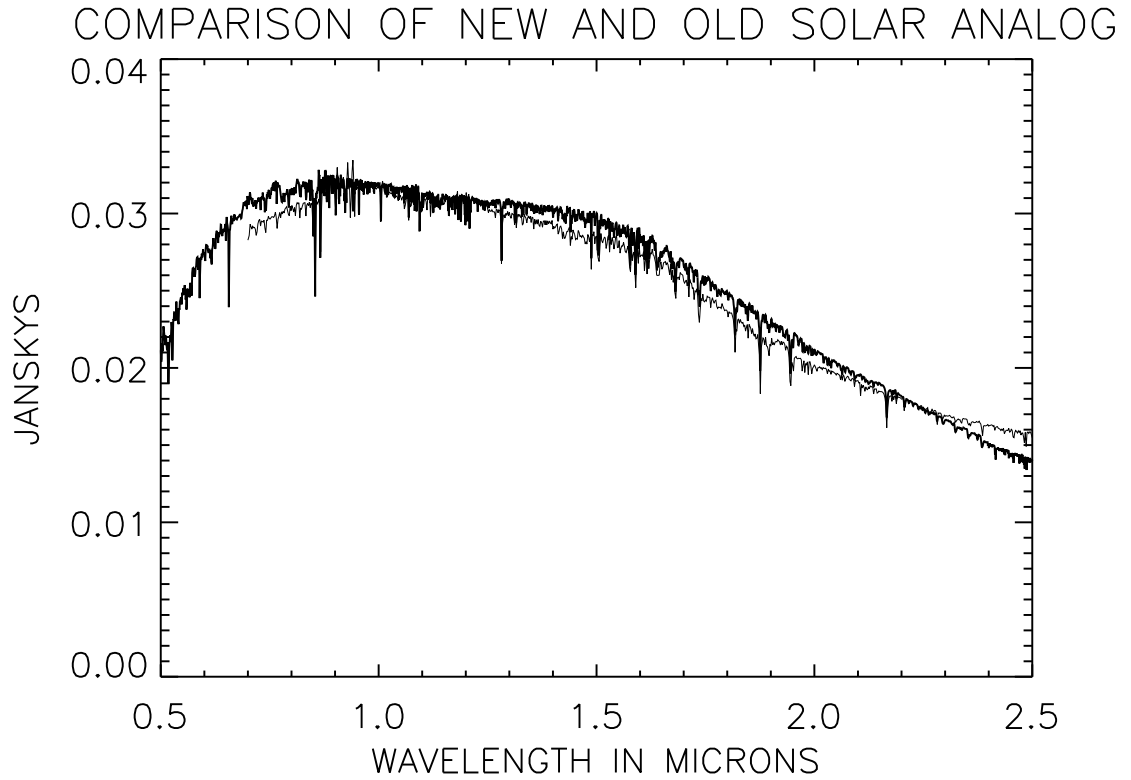


Figure 3: Comparison between the solar spectrum from Thuillier et al. 2003 (thick line) and the old solar analog spectrum (thin line).

Table 3: The aperture functions for the NICMOS Camera 2 F110W and F160W filter for a solar spectrum star. The aperture sizes are in arc seconds.

Filter/Ap.	0.54	1.0	1.6	3.0	6.0
F110W	0.700	0.889	0.950	0.990	1.0
F160W	0.645	0.856	0.924	0.978	1.0

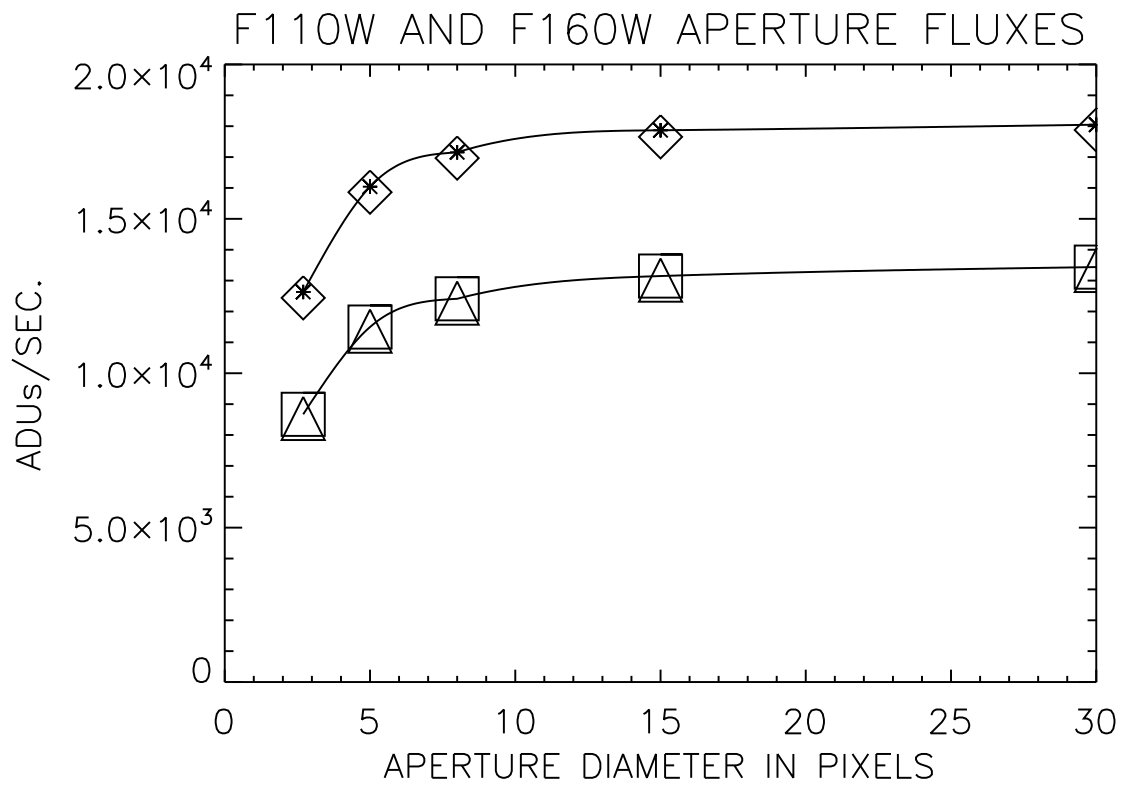


Figure 4: The F110W and F160W aperture functions. The diamonds and asterisks are the average and median F110W fluxes. The triangles and squares are the F160W average and median fluxes.

in those apertures and they should be increased by the inverse of the aperture function to account for the full flux when comparing the flux in the apertures relative to the ACS flux. Aperture corrections for the ACS observations are given in Sirianni et al. (2005).

12. Possible Non-Linearity

The possibility of a non-linear response in NICMOS observations has been raised in this workshop. Refer again to the contributions by deJong and Mobasher. At the time of this submission the author has not been able to independently check the validity of this effect but users of the catalog should be aware of the possibility of its existence. After this check is completed the author expects to submit a version 3 of the NHUDF observations to MAST taking into account all of the calibration issues discussed here.

Acknowledgments. This paper is based on data from observations with the NASA/ESA Hubble Space Telescope, obtained at STScI which operated by the Association of Universities for Research in Astronomy, Inc., under NASA contract NAS 5-26555.

References

- Bessell, M. S. 1990, *PASP*, 102, 1181
Campins, H., Rieke, G. H. & Lebofsky, M. J. 1985, *AJ*, 90, 896
Mobasher et al. 2004, *HST Data Handbook for NICMOS*, version 6.0, (Baltimore: STScI),
<http://www.stsci.edu/hst/nicmos/documents/handbooks/DataHandbookv6>
Persson, S. E. et al. 1998, *AJ*, 116, 2475
Sirianni, M. et al. 2005, *PASP* 117, 1049
Thompson, R. I. et al. 2005, *AJ*, 130, 1
Thuillier, G. et al. 2003, *Solar Physics*, 214, 1